Tunneling of two bosonic atoms from a one-dimensional anharmonic trap

I. S. Ishmukhamedov[1,2,*] and V. S. Melezhik[1,3,†]

[1]*Bogoliubov Laboratory of Theoretical Physics, Joint Institute for Nuclear Research, Dubna, Moscow Region 141980, Russian Federation*

[2]*Al-Farabi Kazakh National University, Almaty 050040, Kazakhstan*

[3]*Peoples' Friendship University of Russia (RUDN University), 6 Miklukho-Maklaya Street, Moscow 117199, Russian Federation*

(Received 25 January 2017; published 6 June 2017)

We investigate the quantum dynamics of two interacting bosonic atoms confined in a one-dimensional anharmonic trap. The tunneling rate, an experimentally measurable parameter of the system, is calculated as a function of the effective coupling interatomic constant g from the ground ($n = N = 0$) and first excited atomic states in the trap with respect to relative ($n = 2, N = 0$) and center-of-mass ($n = 0, N = 2$) atomic motion. This allows us to investigate the initial population and pair correlation, as well as the effective coupling constant g, of the system by comparing the calculated tunneling rate with the experimental one. We observe that the only possible tunneling scenario is a sequential particle tunneling in the cases we consider. We also analyze a rearrangement $(0,2) \rightleftarrows (2,0)$ of the spectrum in the limit $g \to \pm 0$ of noninteracting atoms.

DOI: 10.1103/PhysRevA.95.062701

I. INTRODUCTION

One of the basic effects of quantum mechanics, a particle tunneling through a repulsive barrier, responsible for such fundamental processes as α decay and nuclear fission and fusion, has attracted in recent years a great deal of attention in connection with the cold-atom simulation of different phenomena from solid state to nuclear and high-energy physics. In particular, in recent experiments [1] aspects of atomic tunneling through the walls of confining traps such as pairing and BCS-BEC crossover (from a Bardeen-Cooper-Schrieffer pairing to a Bose-Einstein condensate) have been investigated. Also attributable to this class of problems are tunneling of a BEC [2] and ultracold bosonic few-body systems [3,4], a simulation with ultracold atoms of tunneling processes stimulated by ultrashort intense laser fields [5], transport of the repulsive BEC, and modeling of the Josephson effect in a double-well trap [6]. In Refs. [1,7] it was shown that a tunneling rate through the walls of atomic traps is an experimentally measurable parameter containing important information about the atomic dynamics inside the trap as well as the initial state of the quantum system. However, to extract this information one has to perform a corresponding accurate calculation of the tunneling rate for comparison with the experimental one.

So far, a theoretical description of the tunneling dynamics through repulsive barriers of different form is a quite nontrivial task. In modern computations a semiclassical Wentzel-Kramers-Brillouin (WKB) approach remains the basic analytical method despite its known shortcomings [8,9]. The main disadvantage here is that the WKB method completely neglects interparticle interactions and therefore can produce significant errors in the end results [10]. Therefore, to treat different tunneling dynamics, which depends on the specific peculiarities of each problem, a variety of numerical approaches was developed during the past two decades in atomic, molecular, and nuclear physics [10–15].

In the present work we investigate the tunneling dynamics of two interacting bosonic atoms through the walls of a one-dimensional (1D) anharmonic trap by using an extension of the computational splitting-up technique suggested in [11] for ionization of hydrogenlike atoms by strong electric fields. With this approach we calculate the dependence of the tunneling rate from the first three low-lying atomic states in a confining trap on the effective coupling constant g. The rates of the transitions between the states are also investigated. The obtained results can be used to recover the physical picture inside the confining trap by comparing the calculated tunneling rates with the experimental ones. Similar tunneling processes were qualitatively investigated for tunneling through a box-shaped potential model from the ground state of a rectangular potential well [16].

The paper is organized as follows. In Sec. II we define the Hamiltonian of the two-atom system confined in a 1D anharmonic trap. Key points of the splitting-up method are given in Sec. III for numerical integration of the 2D time-dependent Schrödinger equation describing the two-body quantum dynamics in a 1D anharmonic atomic trap. Special attention is paid to the stable and accurate procedure of extracting the tunneling rate of the system. The obtained results of the calculation of the tunneling rates and transition probabilities are given and discussed in Sec. IV. We also discuss a rearrangement of the spectrum of the two confined atoms in the limit $g \to \pm 0$ of noninteracting atoms. Finally, in Sec. V we draw our conclusions and provide a short outlook.

II. PROBLEM FORMULATION

A. Interaction potentials

The quantum dynamics of two identical bosonic atoms with masses m in a 1D confining trap $\sum_{j=1,2} V(x_j)$ is described by the following Hamiltonian:

$$H = -\frac{\hbar^2}{2m}\frac{\partial^2}{\partial x_1^2} - \frac{\hbar^2}{2m}\frac{\partial^2}{\partial x_2^2} + V(x_1) + V(x_2) + V_{\rm int}(x_1 - x_2), \tag{2.1}$$

*i.ishmukhamedov@mail.ru

†melezhik@theor.jinr.ru

TABLE I. Trap parameters from the Haller *et al.* experiment [20].

Parameter	Value
trap frequency ω	$2\pi\times 14.5$ kHz
wavelength λ	$1.064\,49\times10^{-4}$ cm
anharmonicity α	$-0.030\,455\,2$

where the interatomic potential $V_{\rm int}(x_1-x_2)$ is chosen in the Gaussian form

$$V_{\rm int}(x_1-x_2)=-V_0\exp\left\{-\frac{(x_1-x_2)^2}{2r_0^2}\right\}, \tag{2.2}$$

with the depth V_0 and r_0 defining the range of the interaction. The Hamiltonian (2.1) can be considered as an effective Hamiltonian describing the dynamics of two atoms tightly confined in the transverse direction (y,z) (atomic motion is forbidden in the transverse direction) but with a softer confinement in the longitudinal direction x described by a standing-wave form [17,18]

$$V(x_j)=V_{\rm d}\sin^2\left(\frac{2\pi}{\lambda}x_j\right),\quad j=1,2. \tag{2.3}$$

The interaction of the atom j with the optical trap (2.3) is defined by the wavelength λ of the external laser field and the atomic polarizability (included in the parameter $V_{\rm d}$) [17,18]. Here we use the parametrization of Refs. [17,19],

$$V(x_j)=-\frac{\hbar\omega}{12\alpha}\sin^2\left(\sqrt{-6\alpha}\frac{x_j}{\ell}\right),\quad j=1,2, \tag{2.4}$$

where the parameter of anharmonicity $\alpha=-\frac{8\pi^2\hbar}{12\lambda^2 m\omega}$ and ω and ℓ, defined as $\omega=\frac{2\pi}{\lambda}\sqrt{\frac{2|V_{\rm d}|}{m}}$ and $\ell=\sqrt{\frac{\hbar}{m\omega}}$, were introduced.

To have a realistic scale for the atom-trap interaction (2.4) we use the parameters λ and ω corresponding to the optical traps from the experiment in [20], where confined ^{133}Cs atoms were investigated (see Table I). In the present work we restrict ourselves to the consideration of the atomic dynamics in the single well of the 1D lattice (2.4) by approximating the latter as

$$V^{(\rm SW)}(x_j)=\begin{cases}-\frac{\hbar\omega}{12\alpha}\sin^2\left(\sqrt{-6\alpha}\frac{x_j}{\ell}\right), & |x_j|\leqslant\frac{\pi\ell}{\sqrt{-6\alpha}}\\ 0, & |x_j|>\frac{\pi\ell}{\sqrt{-6\alpha}},\end{cases} \tag{2.5}$$

where $j=1,2$. Such an approximation neglects the tunneling of the atoms through the walls of the 1D lattice neighbor to the single-well trap as well as the reflection from the walls (see Fig. 1).

B. Initial-state preparation

A modern experimental setup permits a preparation of the well-defined and practically nondecaying initial atomic states in confining traps with the subsequent "switching on" of the tunneling process by means of a narrowing of the width of the confining potential [1,7]. To model such a process [10], first we prepare the nondecaying initial atomic bound state at $t\leqslant 0$ by solving the eigenvalue problem for the potential

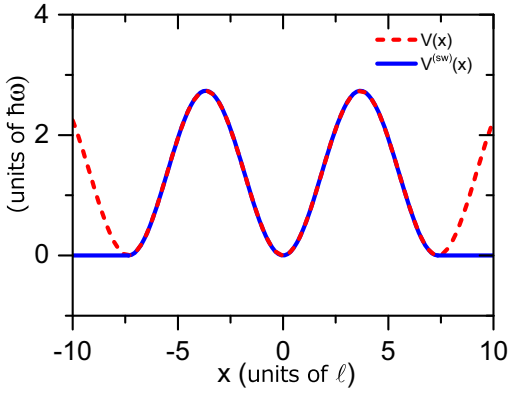

FIG. 1. Approximation (2.5) (blue solid curve) of the exact trap potential (2.4) (red dashed curve) for $\alpha=-0.030\,455\,2$.

$V_{\rm int}(x_1-x_2)+\sum_{j=1,2}V^{(6)}(x_j)$ with the confining trap [21,22]

$$V^{(6)}(x_j)=\hbar\omega\left[\frac{1}{2}\left(\frac{x_j}{\ell}\right)^2+\alpha\left(\frac{x_j}{\ell}\right)^4+\frac{4\alpha^2}{5}\left(\frac{x_j}{\ell}\right)^6\right],\quad j=1,2 \tag{2.6}$$

having an infinite width of the walls and repeating the form of the internal part of the confining potential (2.5) $V^{(\rm SW)}(x_j)$. At $t>0$, the trap $V^{(6)}(x_j)$ is replaced by $V^{(\rm SW)}(x_j)$ to allow the atoms to tunnel out of it. A plot of the potentials $V^{(\rm SW)}(x_j)$ and $V^{(6)}(x_j)$ is presented in Fig. 2.

III. METHOD

To calculate a tunneling rate γ from the bound state of the potential $V_{\rm int}(x_1-x_2)+\sum_{j=1,2}V^{(\rm SW)}(x_j)$ we integrate the 2D time-dependent Schrödinger equation

$$i\hbar\frac{\partial\psi(x_1,x_2,t)}{\partial t}=H(x_1,x_2)\psi(x_1,x_2,t) \tag{3.1}$$

with the Hamiltonian $H(x_1,x_2)$ defined by Eqs. (2.1), (2.2), and (2.5). Based on ideas from [23], which were developed in

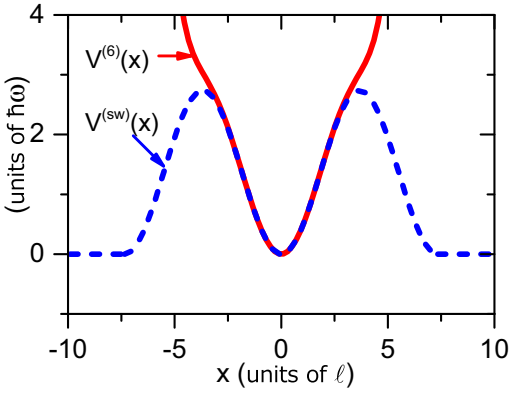

FIG. 2. Initial confining trap $V^{(6)}(x)$ (red solid curve), which confines the motion of the atoms at $t\leqslant 0$, and a modified trap $V^{(\rm SW)}(x)$ (blue dashed curve), which releases the atoms due to quantum tunneling at $t>0$.

Refs. [24,25] in application to confined ultracold atom-atom collisions in waveguidelike traps, we employ the component-by-component split-operator method to integrate Eq. (3.1):

$$\psi(x_1,x_2,t+\Delta t) = \exp\left\{-i\frac{\Delta t}{2\hbar}V_{\rm int}(x_1-x_2)\right\} \times \exp\left\{-\frac{i\,\Delta t\,H_1(x_1)}{\hbar}\right\}\exp\left\{-\frac{i\,\Delta t\,H_2(x_2)}{\hbar}\right\} \times \exp\left\{-i\frac{\Delta t}{2\hbar}V_{\rm int}(x_1-x_2)\right\}\psi(x_1,x_2,t), \tag{3.2}$$

where

$$H_j(x_j) = -\frac{\hbar^2}{2m}\frac{\partial^2}{\partial x_j^2} + V^{(\rm SW)}(x_j), \quad j=1,2. \tag{3.3}$$

The computational scheme (3.2) is correct up to terms of $O(\Delta t^3)$. Following [24,25], we approximate the action of the differential operators $\exp\{-i\,\Delta t/\hbar H_j(x_j)\}$ by an implicit Crank-Nicolson scheme

$$\exp\left\{-\frac{i\,\Delta t\,H_j(x_j)}{\hbar}\right\} = \left(1+\frac{1}{2\hbar}i\,H_j\,\Delta t\right)^{-1}\left(1-\frac{1}{2\hbar}i\,H_j\,\Delta t\right),$$

which maintains the accuracy of the split-operator method (3.2).

The finiteness of the width of the confining potential wall causes a broadening of the energy levels in the potential describing the interatomic and atom-trap interactions $V_{\rm int}(x_1-x_2)+\sum_{j=1,2}V^{(\rm SW)}(x_j)$ due to atom tunneling through the wall of the confining trap. This means that we need to have an outgoing wave away from the region of action of the confining potential, i.e., at $x_1,x_2\to\pm\infty$ [14,26]. This kind of boundary condition in the time-dependent scheme can be modeled by introducing at the edge of the radial grid x_m some type of an *absorber* [26] or a mask function [27]. Here we choose the scheme with the additional complex absorbing potential (CAP) near the edge of the radial grid in the form suggested in [15,26],

$$W(x_j) = w_c(|x_j|-x_c)^2\theta(|x_j|-x_c), \quad j=1,2, \tag{3.4}$$

where $\theta(x)$ is the Heaviside step function and the parameter x_c defines a region where the CAP switches on and it should be chosen at a point behind the barrier of the confining potential $V^{(\rm SW)}$. The choice of the parameter w_c is discussed in the paragraph after Eq. (3.6). A plot of the CAP (3.4) with the confining potential $V^{(\rm SW)}$ (2.5) is shown in Fig. 3.

The numerical integration of the Schrödinger equation (3.1) with the Hamiltonian $H(x_1,x_2)=\sum_{j=1,2}[H_j(x_j)+iW(x_j)]+V_{\rm int}(x_1-x_2)$ defined by (3.3), (2.5), (3.4), and (2.2) permits us to extract the desired tunneling rate γ (or the energy level width $\Gamma=\hbar\gamma$) from the decay of the total probability

$$P(t) = \int_{-x_m}^{x_m}\int_{-x_m}^{x_m} dx_1dx_2|\psi(x_1,x_2,t)|^2 \sim \exp\{-\gamma t\} \tag{3.5}$$

to find the atoms in the box $|x_1,x_2|\leqslant x_m$, i.e., the total population of the atomic bound states in the box. From

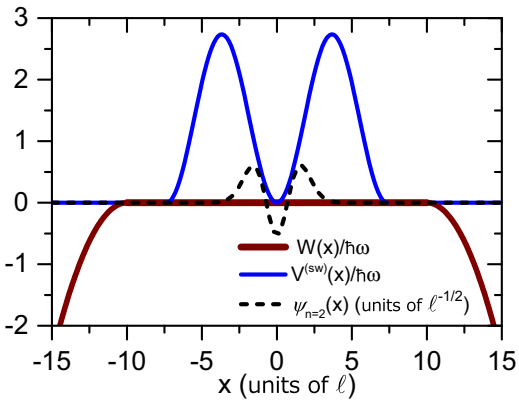

FIG. 3. Plot of the absorbing potential $W(x)$ (3.4) (thick red solid curve) and the confining potential $V^{(\rm SW)}(x)$ (2.5) for $\alpha=-0.030\,455\,2$ (blue solid curve). We also plot the wave function $\psi_{n=2}(x)$ (black dashed curve) of the first even excited state in the confining potential to illustrate the scale of the problem.

Eq. (3.5) one can define the tunneling rate as

$$\gamma = -\frac{1}{P(t)}\frac{dP(t)}{dt}. \tag{3.6}$$

The determination of the tunneling rate from (3.6) obviously holds only for the exponential decay of the probability (3.5). This condition restricts the choice of the parameters x_c and w_c of the CAP (3.4) as well as the time domain where the decay of the norm (3.5) is stabilized after the beginning of the tunneling [11]. Here we choose $x_c=10\ell$ and $w_c=-0.1\hbar\omega\ell^{-2}$ from a domain where the tunneling rate γ is independent, to a good accuracy, of the variation of these parameters.

Following the pioneering works in [28,29], which laid the foundation for investigations of the confined two-body systems in a quasi-1D geometry of atomic traps, we define here the interatomic interaction through the effective coupling constant g connected with the 1D scattering length $a_{\rm 1D}$ as

$$g = -\frac{2\hbar^2}{ma_{\rm 1D}}. \tag{3.7}$$

The scattering length $a_{\rm 1D}$ was calculated by the integration of the 1D Schrödinger equation

$$\left[-\frac{\hbar^2}{2\mu}\frac{d^2}{dx^2}+V_{\rm int}(x)\right]\psi_{\rm sc}(x) = \frac{\hbar^2k^2}{2\mu}\psi_{\rm sc}(x), \tag{3.8}$$

describing the atom-atom collision in 1D free space, with the boundary condition

$$\psi_{\rm sc}(x) \xrightarrow[x\to\pm\infty]{} \cos[k|x|+\delta(k)] \tag{3.9}$$

at the zero-energy limit $k=\sqrt{2\mu E}/\hbar\to 0$. The calculated scattering phase $\delta(k)$ defines at $k\to 0$ the 1D scattering length

$$a_{\rm 1D} = \lim_{k\to 0}\frac{\cot[\delta(k)]}{k}. \tag{3.10}$$

Here $\mu=m/2$ and $x=x_1-x_2$ are the reduced mass and the relative coordinate of the atomic pair, respectively.

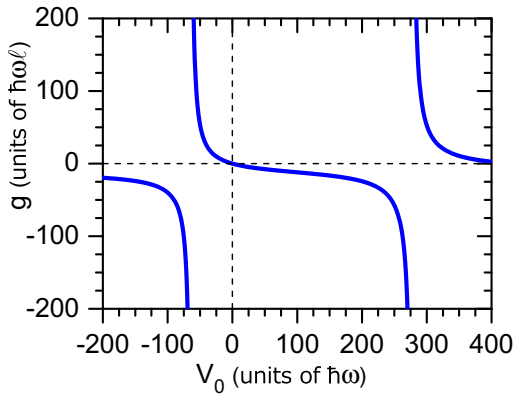

FIG. 4. Dependence of the effective coupling constant g on the depth V_0 of the interaction potential (2.2) (blue solid line) at $r_0 = 0.1\ell$.

The dependence of the coupling constant g on the depth V_0 of the interaction potential $V_{\rm int}$ (2.2), calculated at $r_0 = 0.1\ell$, is shown in Fig. 4. The choice of the parameter r_0, fixed in [10,30], adequately corresponds to current experiments [1,7,20] where the range of the confining potential ℓ always essentially exceeds the range of the interatomic interaction: $r_0 \ll \ell$.

In the calculations, the parameter V_0 varied in the range $-64 \lesssim V_0/\hbar\omega \lesssim 53$, which corresponds to $+\infty \gtrsim g/\hbar\omega\ell \gtrsim -8$. It has permitted us to investigate the tunneling processes in a wide range of coupling strength g from an attraction $g < 0$ to a strong repulsion $g \to +\infty$

IV. RESULTS

A. Energy spectrum of the system in a nondecaying initial state

In Fig. 5 we present the energy spectrum of two bosonic atoms calculated as a function of the coupling constant g in the confining potential $V^{(6)}(x_j)$ (2.6) and in the harmonic trap $V^{(2)}(x_j)$ corresponding to the case $\alpha = 0$. For an identification of the calculated states of the spectrum we use quantum

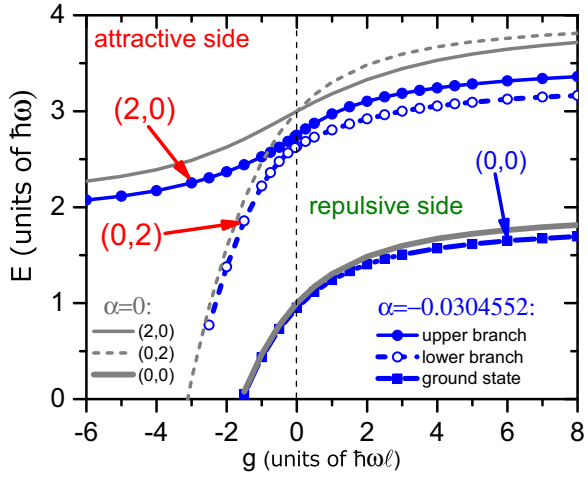

FIG. 5. Three lowest energy levels of two bosonic atoms as a function of the coupling constant g in the confining potential $V^{(6)}(x_j)$ with $\alpha = -0.030\,455\,2$ (blue curves) and in the harmonic trap $V^{(2)}(x_j) = \frac{1}{2}m\omega^2 x_j^2$ (gray curves).

numbers n and N characterizing the quantization (induced by the trap) of the relative and center-of-mass atomic motions, respectively, which are good ones in the harmonic limit [i.e., when $\alpha = 0$ in (2.6)] due to the separation of the relative and center-of-mass atomic variables. In Fig. 5 the three lowest states of the calculated spectrum are presented: the ground state ($n = 0, N = 0$) and the first two excited states (0,2) and (2,0). We define the quantum numbers (n,N) of the two-atom state inside the trap by the nodal structure of the calculated wave function $\psi_{n,N}(x,y,t=0)$ with respect to the variables of the relative $x = x_1 - x_2$ and center-of-mass $y = (x_1 + x_2)/2$ motions.

The analysis of the nodal structure of the wave function $\psi_{n,N}(x,y,t=0)$ given in Sec. IV C shows that the first excited state at negative g is (0,2) and the second one is (2,0). When $\alpha = 0$ the energy branches (0,2) and (2,0) cross each other at zero coupling $g = 0$ (noninteracting atoms). This corresponds to a pure two-dimensional harmonic oscillator and these levels become degenerate due to rotational symmetry. This symmetry breaks if $\alpha \neq 0$ and we observe an avoided crossing of these energy levels at $g = 0$. Moreover, at positive g, the first excited state becomes (2,0) and the second one (0,2), i.e., we observe a rearrangement (0,2) $\rightleftarrows$ (2,0) of the spectrum in the limit $g \to \pm 0$.

B. Tunneling dynamics from bound states of the two-atom confined system

By numerically integrating the 2D time-dependent Schrödinger equation (3.1) for $t > 0$, we calculate the time evolution (3.2) of the two-atom wave packet $\psi_{n,N}(x,y,t)$ from the ground (0,0) and the excited states (0,2) and (2,0) as a function of the coupling constant g. In the calculation the sixth-order finite-difference approximation on the uniform spatial grid over x_1 and x_2 was used [24,25]. The range $|x_j| \leqslant x_m$ of the space of radial variables was chosen as $x_m = 20\ell$ and the steps of integration over radial variables as well as the steps of integration over the time $\Delta t = 0.01\omega^{-1}$ were chosen to keep the accuracy of the calculation of the tunneling rates within the order of 1%.

1. Ground state

First we calculated the tunneling rate γ from the ground state (0,0) as a function of the coupling constant g for a fixed parameter of the anharmonicity $\alpha = -0.030\,455\,2$. The tunneling rates γ were extracted from the calculated dependence on time of the total probability $P(t)$ (3.5) with the help of Eq. (3.6). The result of the calculations are presented in Figs. 6(a) and 7. Figure 7 demonstrates excellent agreement of the calculated time dependence of the probability $P(t)$ with Eq. (3.5) at $t \gtrsim 1$ ms. The agreement qualitatively persists in all the considered range of variation of the coupling constant g. This circumstance permitted us to use Eq. (3.6) to extract the tunneling rates given in Fig. 6.

In Fig. 6 we observe rather week monotonic grow of the tunneling rate γ with increasing coupling constant g. The rate γ reaches a finite asymptotic value $\gamma \to 2.6\,\mathrm{s}^{-1}$ in the limiting case of a resonantly strong interaction $g \to +\infty$ (see Fig. 7). This week dependence of the rate γ on the coupling constant g is understood due to the sufficiently large thickness of the walls

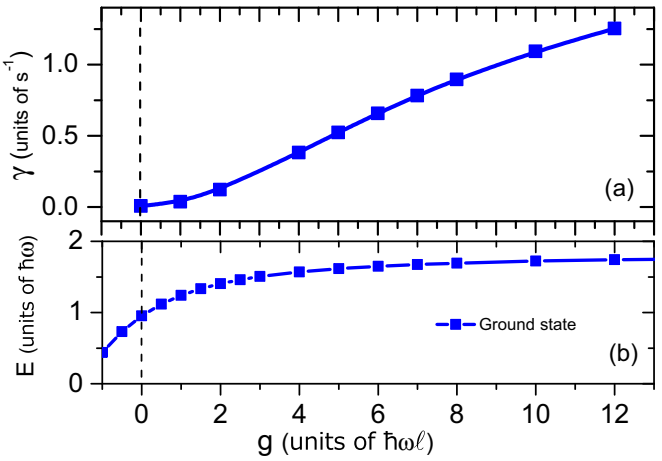

FIG. 6. (a) Tunneling rate γ from the ground state as a function of the coupling constant g and (b) the corresponding energy of the initial state in the closed trapping potential (2.6) with $\alpha = -0.030\,455\,2$.

of the confining potential in the ground state when compared with excited states.

2. *Excited states*

In Fig. 8(a) we present the tunneling rates γ calculated with (3.5) and (3.6) from the first two excited states (0,2) and (2,0) for a wide range of variation of the coupling constant g. The corresponding eigenenergies of the initial state for the trap potential $V^{(6)}(x_j)$ (2.6) are also shown in Fig. 8(b).

a. Upper energy branch of the excited states. Figure 9 demonstrates the calculated time evolution of the total probabilities $P(t)$ (3.5) decaying from the upper branch of excited-state energy levels presented in Fig. 8(b) and the corresponding tunneling rates $\gamma(t)$ (3.6). Here one can observe a quite fast transition of the decay of the total probabilities $P(t)$ to the exponential law as well as a fast convergence of the tunneling rates $\gamma(t)$ to the limiting value $\gamma(t) \to \gamma(\infty)$ for a wide range of variation of the coupling constant g. One should notice a dramatic change of the tunneling rate γ in Fig. 9 with the change of g. It is also reflected in Fig. 8(a), where one can observe a nonmonotonic dependence of the tunneling rate γ

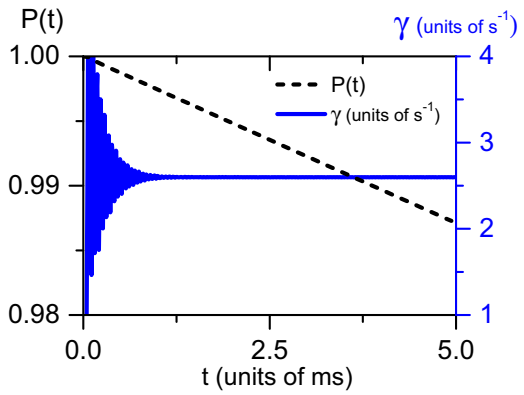

FIG. 7. Tunneling rate γ (blue solid curve) and the total probability $P(t)$ (black dashed curve) from the ground state at $g \to \infty$.

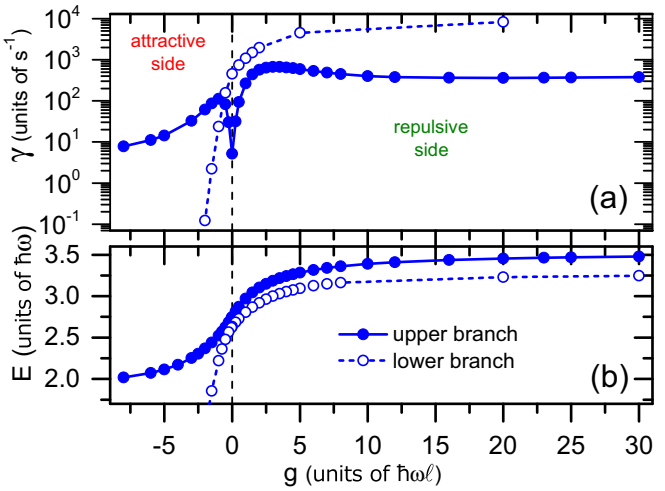

FIG. 8. (a) Tunneling rates from the first two excited states as a function of the coupling constant g for $\alpha = -0.030\,455\,2$. (b) Energies of the first two excited states in the closed trapping potential (2.6) with $\alpha = -0.030\,455\,2$ as a function of the coupling constant g.

on the coupling constant g. The origin of this effect is explained in Sec. IV C.

To understand the mechanism of tunneling from the upper energy branch of the excited states we also calculate the

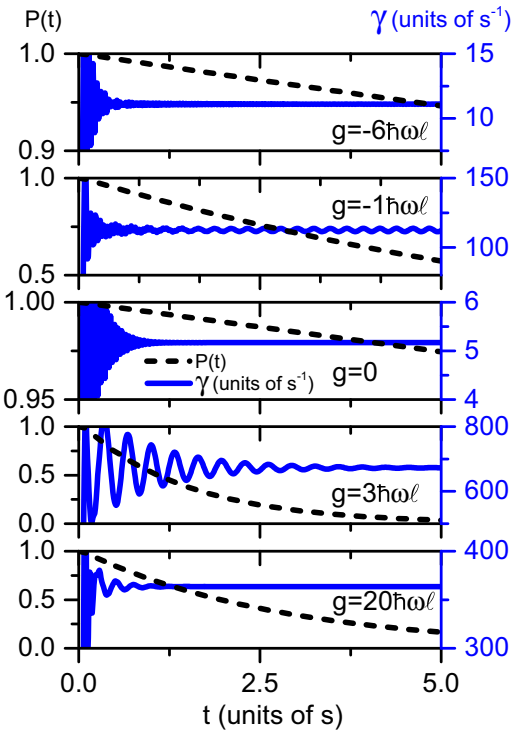

FIG. 9. Time evolution of the total probability $P(t)$ (black dashed curves) from the upper branch of excited-state energy levels presented in Fig. 8(b) and the corresponding tunneling rates γ (blue solid curves). Calculations were performed for a few values of the coupling constant: $g/\hbar\omega\ell = -6, -1, 0, 3, 20$.

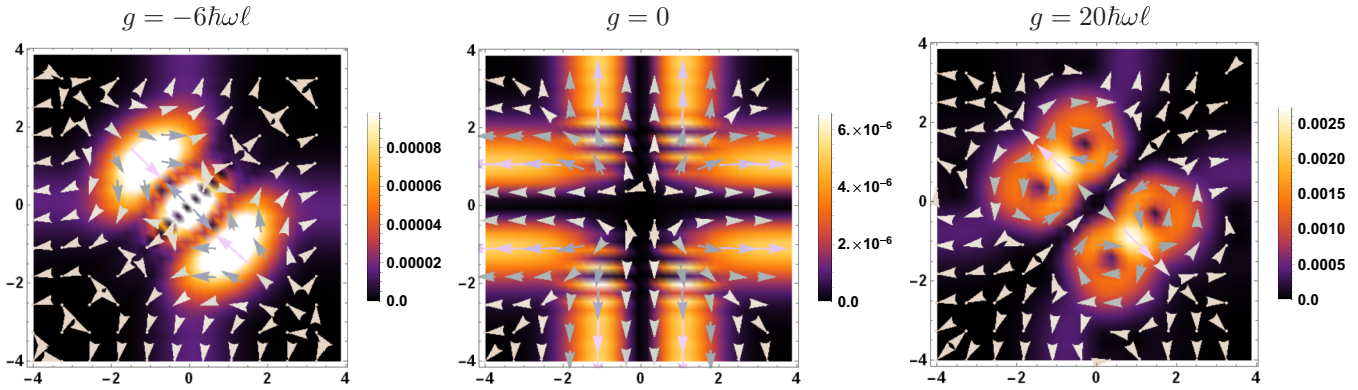

FIG. 10. Distribution of a modulus of the flux $|\mathbf{j}(x_1,x_2,t)|$ (in $\omega\ell^{-1}$ units) from the upper branch of the excited states presented in Fig. 5 [or equivalently in Fig. 8(b)] and its direction (in arbitrary units) for different values of the coupling constant g at $t = 120\omega^{-1} \approx 1.32$ ms.

probability current density $j_k(x_1,x_2,t)$,

$$j_k(x_1,x_2,t) = \frac{\hbar}{2mi}\left(\psi^*\frac{\partial\psi}{\partial x_k} - \psi\frac{\partial\psi^*}{\partial x_k}\right), \quad k = 1,2, \qquad (4.1)$$

at a certain time t. In Fig. 10 the fluxes $|\mathbf{j}(x_1,x_2,t)|$, calculated for different values of the coupling constant g, are presented.

From Fig. 10 we see that the flux in all of the cases shows a complicated behavior near the origin $x_1 = x_2 = 0$. What all the graphs in Fig. 10 have in common is that the dominant flux directions are along the axes x_1 and x_2. This corresponds to a single-particle tunneling.

To analyze the mechanism of the tunneling more quantitatively we divide (following [14]) the whole space of radial variables (x_1,x_2) into several regions (see Fig. 11) and calculate partial probabilities P_k to find the atom or atomic pair in each region k,

$$P_k(t) = \iint_{\text{region } k} dx_1 dx_2 |\Psi(x_1,x_2,t)|^2, \quad k = 1,2,3,4. \qquad (4.2)$$

Detection of the atom in regions 3 corresponds to a sequential single-particle tunneling from the trap and the detection in regions 1 corresponds to a tunneling of two particles as a bound system. More complicated tunneling to regions 2 was discussed in [14] for an example of the two-proton decay of nuclei. We define the size of region 4 to approximately cover the initial atomic distribution in the confining trap $V^{(6)}$ (2.6), which leads to an estimate of the region as $R = 5\ell$.

The calculated time evolution of the partial probabilities $P_k(t)$ is shown in Fig. 12. Figure 12 demonstrates that the partial probabilities $P_3(t)$ are a few order of magnitude larger than $P_1(t) + P_2(t)$ in all of the cases considered. This clearly shows that the sequential particle tunneling is the dominating mechanism of the tunneling. Due to the smallness of the quantities $P_1(t)$, $P_2(t)$, and $P_3(t)$ in comparison with $P_4(t)$, this latter partial probability approximately equals the total probability $P(t)$ (3.5) and that is why we omit $P_4(t)$ from Fig. 12.

b. Lower energy branch of the excited states. To understand the dynamics of a tunneling process of the atoms bound initially in the lower energy branch of the excited states [Fig. 5 or equivalently Fig. 8(b)] we analyze in detail the case $g/\hbar\omega\ell = 5$ since it captures all the features of such tunneling (see Fig. 13). From Fig. 13 we clearly see that

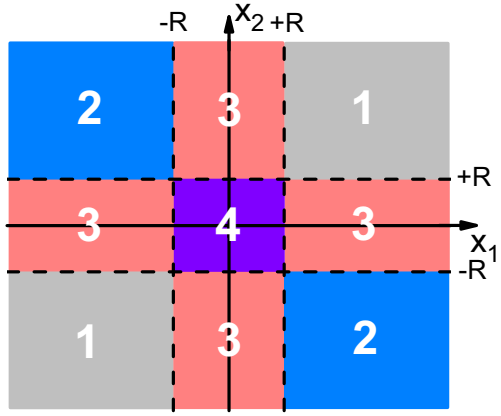

FIG. 11. Division of the radial variable space into several regions for an analysis of the partial probabilities P_k.

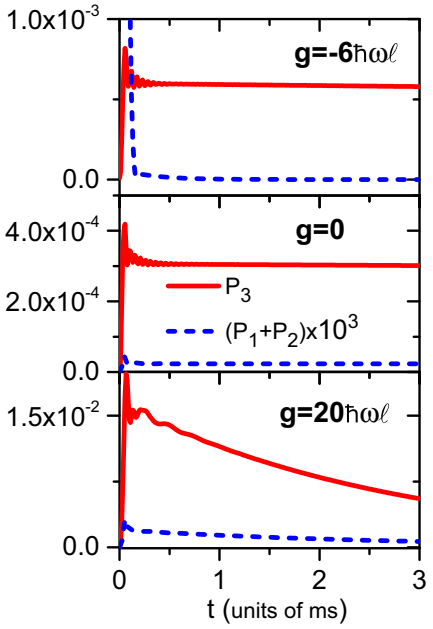

FIG. 12. Partial probabilities $P_k(t)$ (4.2) to populate the regions k for three different values of the coupling constant g.

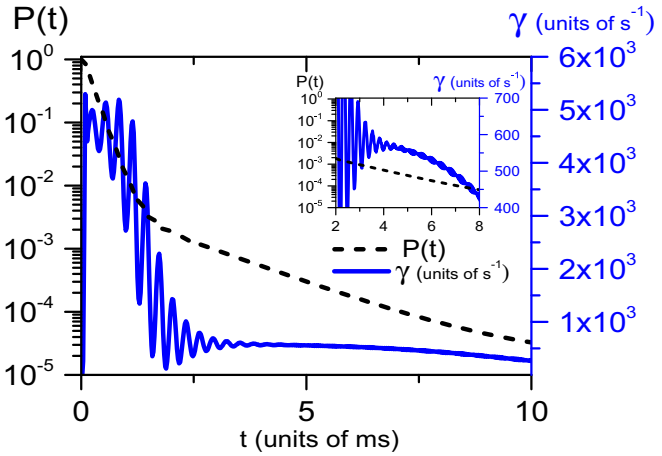

FIG. 13. Tunneling rate γ (blue solid curve) from the lower energy branch of the excited states [shown in Fig. 8(b)] and the corresponding total probability $P(t)$ (black dashed curve) at $g/\hbar\omega\ell = 5$ and $\alpha = -0.030\,455\,2$. The inset shows a close-up of γ and $P(t)$ in the time window $t = 2$–8 ms, which corresponds to the second stage decay (described in the text).

the total probability $P(t)$ decreases in two stages, i.e., we see that the initial exponential behavior of $P(t)$ decreases as $\exp\{-\gamma_1 t\}$, which turns to, approximately at 1.5–2.5 ms, the same exponential law, but now with different tunneling rate $\gamma_1 \to \gamma_2$. The tunneling rate γ_1 calculated with Eq. (3.6) highly oscillates during the first stage of the decay and after approximately $\simeq$1.5–2.5 ms, when the second stage of the decay begins to dominate, the oscillations in $\gamma_2(t)$ significantly damp out, which can be noticed in the inset of Fig. 13.

To extract the tunneling rate γ_1 we fit the total probability $P(t)$ to the exponential function at the time interval $t \leqslant$ 1.5–2.5 ms (see Fig. 14),

$$P_{\text{fit}} = P_0 e^{-\gamma_1 t}. \tag{4.3}$$

By using this fitting procedure we extract the tunneling rate γ_1 of the first decay stage for a wide range of the coupling

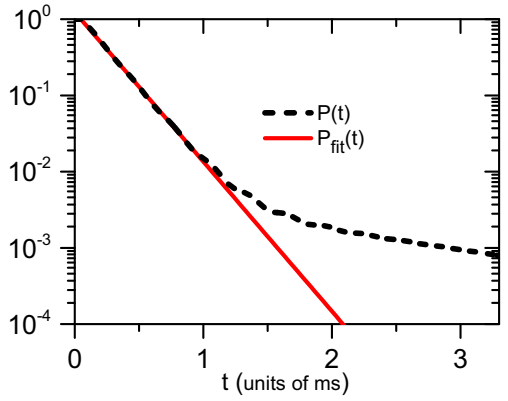

FIG. 14. Total probability $P(t)$ (black dashed curve) and a fitting function (4.3) (red solid line) on a logarithmic scale at $g/\hbar\omega\ell = 5$ and $\alpha = -0.030\,455\,2$. The tunneling rate extracted from the fitting function is about $\gamma_1 \simeq 4520$ s^{-1} in the time window $t = 0.4$–2 ms.

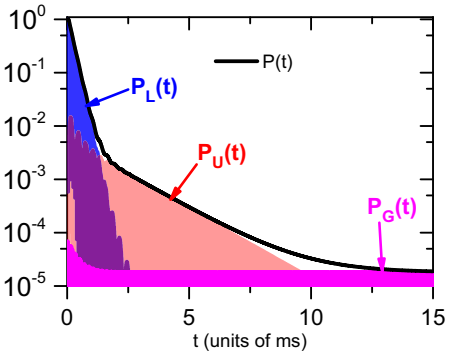

FIG. 15. Time evolution of the populations $P_L(t)$ (blue), $P_U(t)$ (transparent red), $P_G(t)$ (magenta), and the total probability $P(t)$ (black solid curve) to find atoms in the trap, calculated at $g/\hbar\omega\ell = 5$.

constant g. The result of the calculation of the tunneling rate γ_1 is plotted in Fig. 8(a) with open circles.

The tunneling rate γ_2 of the second decay stage from the lower energy branch of the excited states converges to a constant value with increasing time much better than γ_1 but not as good as the tunneling rates from the upper energy branch given in Fig. 9, which can be noticed in the inset of Fig. 13. If we fit the total probability $P(t)$ with the exponential function in the window 2–10 ms we get $\gamma_2 \simeq 580$ s^{-1}. This value approximately coincides with the value of a tunneling rate from the upper energy branch, which equals $\simeq$592 s^{-1} at $g/\hbar\omega\ell = 5$ [see tunneling rates in Fig. 8(a) labeled with closed circles]. To understand this effect we have calculated the time evolution of the populations of the first three low-lying bound states of the two-atom confined system (see Fig. 15) by the formulas

$$\begin{aligned} P_L(t) &= |\langle\psi(x_1,x_2,t)|\psi^{(L)}(x_1,x_2)\rangle|^2, \\ P_U(t) &= |\langle\psi(x_1,x_2,t)|\psi^{(U)}(x_1,x_2)\rangle|^2, \\ P_G(t) &= |\langle\psi(x_1,x_2,t)|\psi^{(G)}(x_1,x_2)\rangle|^2, \end{aligned} \tag{4.4}$$

where $\psi^{(L)}$, $\psi^{(U)}$, and $\psi^{(G)}$ are the wave functions of the two-atom bound system confined in the trap (2.6) at the initial states (at $t = 0$) corresponding to the lower and upper energy branches of the excited states and the ground state, respectively.

From Fig. 15 one can notice that after approximately 2.5 ms, the population $P_U(t)$ of the upper energy branch becomes dominant due to a transition from the lower energy branch. That is, after about 2.5 ms the tunneling goes from the upper energy branch and therefore the value γ_2 of the tunneling rate approaches the tunneling rate from the upper energy branch calculated in the preceding section.

With an increase of time to about 8 ms the populations of the upper energy branch and the ground states become comparable (see Fig. 15) and with a further increase of time the system passes to the ground state, where the tunneling rate is naturally defined by the decay of the ground state. It is interesting that in the case of a very strong interatomic coupling $g \to \infty$ the second stage goes with the tunneling rate that approximately coincides with the tunneling rate from the initial ground state (Fig. 16) due to a faster population of the ground state than the upper energy branch. To see that, one has to compare the inset

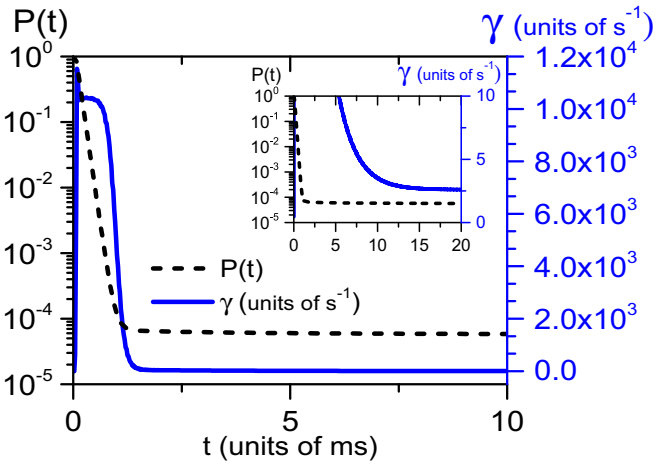

FIG. 16. Tunneling rate γ (blue solid curve) from the lower branch of the excited state [shown in Fig. 8(b)] at $g \to \infty$ and the corresponding total probability $P(t)$ (black dashed curve). The inset shows a convergence $\gamma(t) \to \gamma(\infty)$ to the value, which approximately coincides with γ from the ground state.

of Fig. 16 with the converged result for the tunneling rate γ from the ground state given in Fig. 7.

C. Spectrum rearrangement

In this section we analyze a spectrum rearrangement of two atoms confined in an anharmonic trap $V^{(6)}$ (2.6) at a transition of the special point $g = 0$ of noninteracting atoms with increasing of g from small negative values to small positive values or vice versa. In Fig. 5 we labeled the upper and lower energy branches at the negative side of the coupling constant g with quantum numbers (2,0) and (0,2) correspondingly. These quantum numbers are conserved only at the negative side of the coupling constant g. When these branches cross the point $g = 0$ the nodal structures of these states are rearranged and the states (2,0) and (0,2) are interchanged. With decreasing anharmonic parameter α (see Fig. 17) the effect becomes more pronounced.

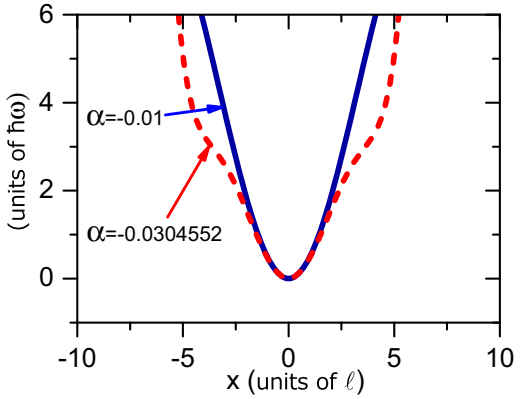

FIG. 17. Confining potential $V^{(6)}(x)$ for two values of the anharmonic parameter α: $\alpha = -0.030\,455\,2$ (red dashed curve) and $\alpha = -0.01$ (blue solid curve).

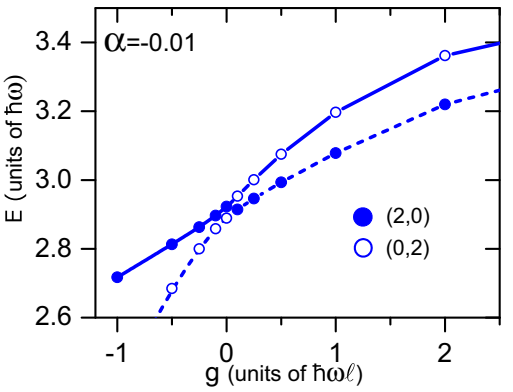

FIG. 18. Pair of energy levels of the first excited states (2,0) (closed circles) and (0,2) (open circles) for two atoms confined in the anharmonic trap $V^{(6)}$ with $\alpha = -0.01$.

Figure 18 shows the calculated energy levels of the pair of first excited states (2,0) and (0,2) for $\alpha = -0.01$. The corresponding wave functions for the two cases $\alpha = -0.01$ and $\alpha = -0.030\,455\,2$ of the upper and lower branches, given in Figs. 18 and 5, respectively, are presented in Figs. 19 and 20, which are plotted as functions of the relative $x = x_1 - x_2$ and center-of-mass $y = (x_1 + x_2)/2$ variables.

From Figs. 19 and 20 we see how the wave functions change their nodal structures when crossing the point $g = 0$: The nodal structure of the upper branch's eigenfunction interchanges between (2,0) and (0,2) states; the same effect occurs for the nodal structure of the lower branch's eigenfunction, only vice versa. A similar effect of the spectrum rearrangement for two atoms confined in a 3D anharmonic trap was observed in [22].

We have also observed some kind of rearrangement of the nodal structure of the calculated wave function in the vicinity of the point $g/\hbar\omega\ell \simeq 3$ at $\alpha = -0.030\,455\,2$ (see Figs. 19 and 20). However, due to the strong interatomic coupling g and considerable anharmonic parameter α we have strong mixing of the states with different quantum numbers and cannot interpret this effect as a simple transition from one state with good quantum numbers (n,N) to another one, like near the point $g = 0$, where the rearrangement of the states $(0,2) \rightleftarrows (2,0)$ occurs.

The calculated dependence of the initial atomic distribution [the probability density $|\psi(x,y,t=0)|^2$] on the coupling constant g clarifies the monotonic increase of the tunneling rate from the lower energy branch of the excited states with an increase of g [Fig. 8(a), open circles]: With the increase of g the maxima of the probability density move closer to regions 3 in Fig. 11 (see Fig. 20).[1] The dependence on g for the tunneling rate from the upper energy branch of the excited states has nonmonotonic character [Fig. 8(a), closed circles] due to the more complicated dependence of the probability density $|\psi(x,y,t=0)|^2$ on g: With a deviation to the left or right of the point $g = 0$ the maxima of the probability density

[1]Figures 19 and 20 show wave functions $\psi(x,y)$, which can be used for analysis of the dependence on g of the maximum of the corresponding density distribution probability $|\psi(x,y,t=0)|^2$.

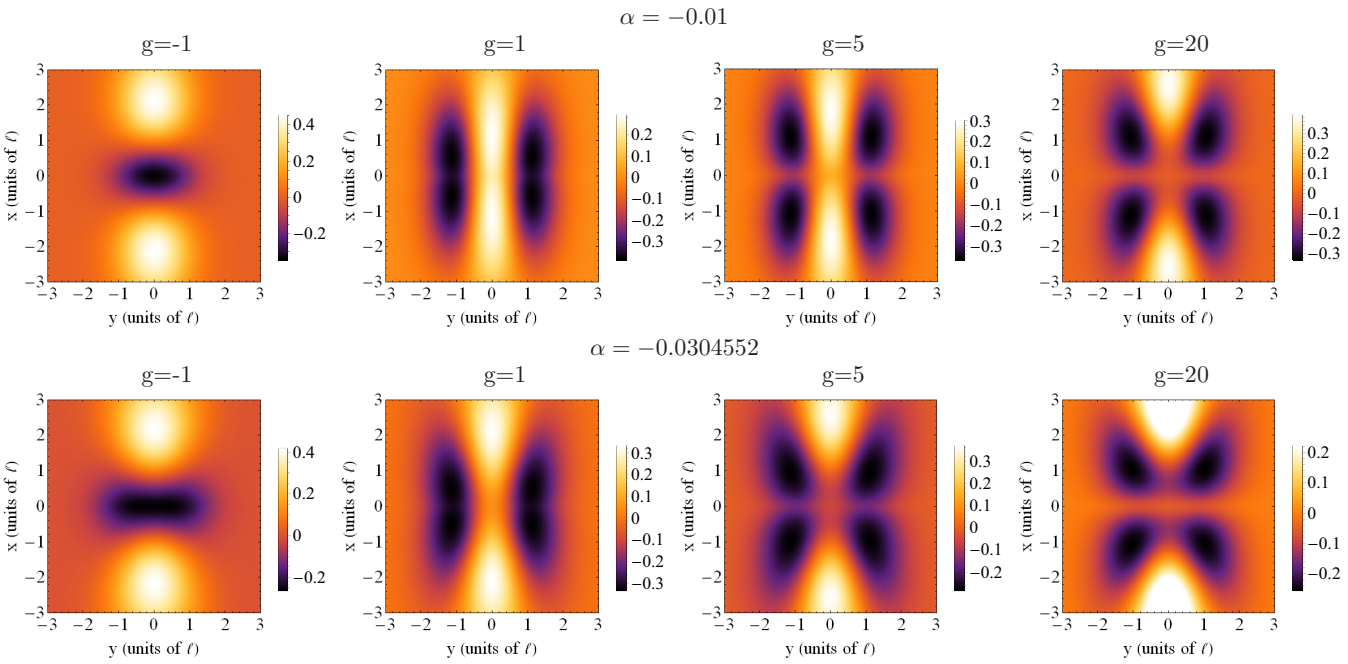

FIG. 19. Wave function $\psi(x,y,t=0)$ (in ℓ^{-1} units) of the upper energy branch. The coupling strength g is in $\hbar\omega\ell$ units.

first approach regions 3 in Fig. 11, but then start to move from regions 3 to region 4 and finally stabilize (see Fig. 19).

V. CONCLUSION

We have investigated the tunneling dynamics of a 1D system of two interacting atoms confined in the anharmonic trap (2.5). We have calculated the tunneling rates γ from the three lowest atomic bound states as a function of the coupling constant g. It was found that in the tunneling from the upper energy branch of the excited states, γ behaves nonmonotonically and the sequential particle channel dominates in the tunneling. Note that the domination of the sequential tunneling was also observed in the box-shaped potential model from the ground state of a rectangular potential well [16]. When the atoms are initially in the lower energy branch of the excited states, γ grows very fast with increasing coupling strength g at the beginning of the tunneling. Then it was found that the tunneling passes to a new regime (or regimes) with a slower tunneling rate (or rates) due to the competition of the tunneling with the

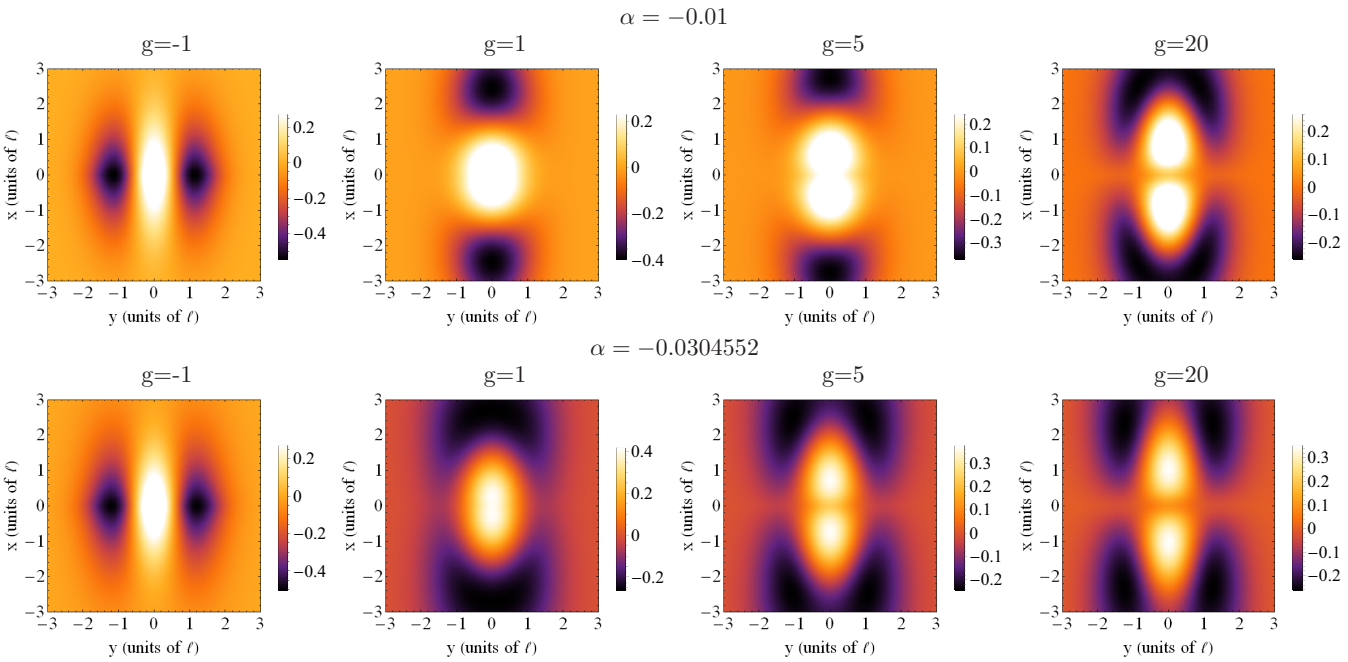

FIG. 20. Wave function $\psi(x,y,t=0)$ (in ℓ^{-1} units) of the lower energy branch. The coupling strength g is in $\hbar\omega\ell$ units.

transition to the upper energy branch of the excited states and to the ground state. When the atoms tunnel from the ground state, γ grows slowly and monotonically with increasing g.

We have also analyzed a rearrangement $(0,2) \rightleftarrows (2,0)$ of the spectrum in the limit $g \to \pm 0$ of noninteracting atoms with the exchange of the wave function's nodal structure. A more complicated rearrangement of the nodal structure of the calculated wave function of the confined pair of atoms was found when crossing the point $g/\hbar\omega\ell \simeq 3$.

The computational scheme developed can be extended to technically more complicated but close to current and planned experiments [1,7], the problem of the tunneling from quasi-1D cigarlike and quasi-2D pancakelike traps. Inclusion of the spin dynamics in the model for the tunneling process is another actual problem that can be investigated with the technique developed.

ACKNOWLEDGMENTS

The authors are very grateful to P. Schmelcher, V. V. Pupyshev, Y. V. Popov, and S. I. Vinitsky for very helpful comments and fruitful discussions. The work was financially supported by the Ministry of Education and Science of the Russian Federation (Agreement No. 02.a003.21.0008) and by a grant of the Plenipotentiary Representative of the Republic of Kazakhstan to JINR.

[1] G. Zürn, A. N. Wenz, S. Murmann, A. Bergschneider, T. Lompe, and S. Jochim, Pairing in Few-Fermion Systems with Attractive Interactions, Phys. Rev. Lett. **111**, 175302 (2013).

[2] R. Beinke, S. Klaiman, L. S. Cederbaum, A. I. Streltsov, and O. E. Alon, Many-body tunneling dynamics of Bose-Einstein condensates and vortex states in two spatial dimensions, Phys. Rev. A **92**, 043627 (2015).

[3] A. U. J. Lode, A. I. Streltsov, O. E. Alon, H.-D. Meyer, and L. S. Cederbaum, Exact decay and tunnelling dynamics of interacting few-boson systems, J. Phys. B **42**, 044018 (2009).

[4] A.U.J. Lode, *Tunneling Dynamics in Open Ultracold Bosonic Systems* (Springer, Heidelberg, 2015).

[5] S. Sala, J. Förster, and A. Saenz, Ultracold-atom quantum simulator for attosecond science, Phys. Rev. A **95**, 011403(R) (2017).

[6] V. O. Nesterenko, A. N. Novikov, and E. Suraud, Transport of the repulsive Bose-Einstein condensate in a double-well trap: Interaction impact and relation to the Josephson effect, Laser Phys. **24**, 125501 (2014).

[7] G. Zürn, F. Serwane, T. Lompe, A. N. Wenz, M. G. Ries, J. E. Bohn, and S. Jochim, Fermionization of Two Distinguishable Fermions, Phys. Rev. Lett. **108**, 075303 (2012).

[8] M. Rontani, Tunneling Theory of Two Interacting Atoms in a Trap, Phys. Rev. Lett. **108**, 115302 (2012).

[9] M. Rontani, Pair tunneling of two atoms out of a trap, Phys. Rev. A **88**, 043633 (2013).

[10] S. E. Gharashi and D. Blume, Tunneling dynamics of two interacting one-dimensional particles, Phys. Rev. A **92**, 033629 (2015).

[11] V. S. Melezhik, A computational method for quantum dynamics of a three-dimensional atom in strong fields, in *Atoms and Molecules in Strong External Fields*, edited by P. Schmelcher and W. Schweizer (Plenum, New York, 1998), pp. 89–94.

[12] P. M. Krassovitskiy and F. M. Pen'kov, Contribution of resonance tunneling of molecule to physical observables, J. Phys. B: At. Mol. Opt. Phys. **47**, 225210 (2014).

[13] A. A. Gusev, S. I. Vinitsky, O. Chuluunbaatar, V. L. Derbov, A. Góźdź, and P. M. Krassovitskiy, Metastable states of a composite system tunneling through repulsive barriers, Theor. Math. Phys. **186**, 21 (2016).

[14] T. Maruyama, T. Oishi, K. Hagino, and H. Sagawa, Time-dependent approach to many-particle tunneling in one dimension, Phys. Rev. C **86**, 044301 (2012).

[15] G. Scamps and K. Hagino, Multidimensional fission model with a complex absorbing potential, Phys. Rev. C **91**, 044606 (2015).

[16] S. Hunn, K. Zimmermann, M. Hiller, and A. Buchleitner, Tunneling decay of two interacting bosons in an asymmetric double-well potential: A spectral approach, Phys. Rev. A **87**, 043626 (2013).

[17] S.-G. Peng, H. Hu, X.-J. Liu, and P. D. Drummond, Confinement-induced resonances in anharmonic waveguides, Phys. Rev. A **84**, 043619 (2011).

[18] I. Bloch, J. Dalibard, and W. Zwerger, Many-body physics with ultracold gases, Rev. Mod. Phys. **80**, 885 (2008).

[19] I. S. Ishmukhamedov, D. T. Aznabayev, and S. A. Zhaugasheva, Two-body atomic system in a one-dimensional anharmonic trap: The energy spectrum, Phys. Part. Nucl. Lett. **12**, 680 (2015).

[20] E. Haller, M. J. Mark, R. Hart, J. G. Danzl, L. Reichsollner, V. Melezhik, P. Schmelcher, and H.-C. Nägerl, Confinement-Induced Resonances in Low-Dimensional Quantum Systems, Phys. Rev. Lett. **104**, 153203 (2010).

[21] S. Grishkevich and A. Saenz, Theoretical description of two ultracold atoms in a single site of a three-dimensional optical lattice using realistic interatomic interaction potentials, Phys. Rev. A **80**, 013403 (2009).

[22] S. Sala and A. Saenz, Theory of inelastic confinement-induced resonances due to the coupling of center-of-mass and relative motion, Phys. Rev. A **94**, 022713 (2016).

[23] G. I. Marchuk, *Methods of Numerical Mathematics* (Springer, New York, 1975), Sec. 4.3.3.

[24] V. S. Melezhik, J. I. Kim, and P. Schmelcher, Wave packet dynamical analysis of ultracold scattering in cylindrical waveguides, Phys. Rev. A **76**, 053611 (2007).

[25] V. S. Melezhik, Mathematical modeling of ultracold few-body processes in atomic traps, EPJ Web Conf. **108**, 01008 (2016).

[26] U. V. Riss and H.-D. Meyer, Calculation of resonance energies and widths using the complex absorbing potential method, J. Phys. B **26**, 4503 (1993).

[27] J. L. Krause, K. J. Schafer, and K. C. Kulander, Calculation of photoemission from atoms subject to intense laser fields, Phys. Rev. A **45**, 4998 (1992).

[28] M. Olshanii, Atomic Scattering in the Presence of an External Confinement and a Gas of Impenetrable Bosons, Phys. Rev. Lett. **81**, 938 (1998).

[29] T. Busch, B. Englert, K. Rzazewski, and M. Wilkens, Two cold atoms in a harmonic trap, Found. Phys. **28**, 549 (1998).

[30] I. S. Ishmukhamedov, D. S. Valiolda, and S. A. Zhaugasheva, Description of ultracold atoms in a one-dimensional geometry of a harmonic trap with a realistic interaction, Phys. Part. Nucl. Lett. **11**, 238 (2014).